Microwave-Assisted Carboxymethylation of Guar Gum Improves Antioxidant and Antibacterial Activity

H.Telli[a,b], H. Maachou[a,b*], Y. Zouambia[a], R. Chebout[c], H. Derdar[d], A-E Hamitouche[c], A.Dekir[e], Y. Larbah[f], Abdullah A. Ghawanmeh[g], Elizabeth A. Brett[h], Aruã C. Da Silva[h*] and Sarah Hudson[h*]

[a] *Laboratory of Materials and Environment (LME), Faculty Technology, University of Medea, Medea 26000, Algeria.*

[b] *Departement of Materials science, Faculty of sciences, University of Medea, Medea 26000, Algeria*

[c] *Scientific and Technical Research Centre in Physico-Chemical Analyses (CRAPC), BP384, Bou-Ismail, Tipaza 42004, Algeria.*

[d] *Laboratory of polymer chemistry (LCP), Department of Chemistry FSEA, University of Oran 1 Ahmed Ben Bella, Oran 31000, Algeria.*

[e] *Laboratory of Applied Organic Chemistry, Synthesis of Biomolecules and Molecular Modelling Group, Sciences Faculty, Chemistry Department, Badji Mokhtar Annaba University, Box 12, 23000 Annaba, Algeria*

[f] *Materials Physics Department, Nuclear Research Centre of Algiers (CRNA),02, Boulevard Frantz Fanon, B.P. 399, Algiers (16000), Algeria*

[g] *Department of Pharmacy, Faculty of Pharmacy, Jadara University, P.O. Box 733, Irbid 21110, Jordan.*

[h] *Department of Chemical Sciences, SSPC the Research Ireland Centre for Pharmaceuticals, Bernal Institute, University of Limerick, Limerick V94 T9PX, Ireland*

** Correspondence to: hamidamaachou@yahoo.fr, Arua.DaSilva@ul.ie and Sarah.Hudson@ul.ie*

Supplementary Information

Table S1: Optimization of reaction parameters of carboxymethylation of one gramme of guar gum by microwave assisted. Green shading highlights the optimal condition. DS – degree of substitution

Mixture	Temperature (°C)	Time of reaction (Min)	MCA (g)	DS Y	Power (W)
1	35	10	0.6	0.249	100
2	35	15	1	0.324	100
3	35	20	1.4	0.457	600
4	50	10	0.6	0.587	600
5	50	20	1.4	0.587	600
6	65	10	0.6	0.598	600
7	65	15	1	0.483	400
8	65	20	1.4	0.591	600
9	35	20	0.6	0.476	400
10	35	20	1	0.567	600
11	35	10	1.4	0.407	400
12	50	20	0.6	0.486	400
13	50	20	1	0.543	600
14	50	15	1	0.64	600
15	65	20	0.6	0.533	600
16	65	20	1	0.605	600
17	65	10	1.4	0.498	400

Cell Culture:

Human dermal fibroblast (HDF) cells were used to assess the biocompatibility of the GG and CMGG. The cells were cultured in Dulbecco's Modified Eagle Medium (DMEM) supplemented with 10% (v/v) fetal bovine serum (FBS) and 1% (v/v) penicillin–streptomycin solution. Cultures were maintained at 37 °C in a humidified atmosphere containing 5% CO_2. The medium was replaced every 2–3 days, and passaging was performed when cells reached approximately 80–90% confluence.

In vitro **cytocompatibility:**

Human dermal fibroblasts (HDFs) were maintained in DMEM supplemented with 10% FBS and 1% penicillin–streptomycin at 37 °C in 5% CO_2. Polymer stocks of GG, CMGG were prepared at 1% (w/v) by dissolving 10 mg polymer in 1 mL sterile deionized water and sterilized by 30 minutes of UV exposure (or 0.22 μm filtration when feasible). Working concentrations (0.01, 0.05, 0.1, 0.5 and 1% w/v) were prepared in culture medium and applied to HDFs seeded at 2×10^3 cells·cm^{-2} in 96-well plates. After 72 h exposure, cell viability was quantified by MTT assay (0.5 mg·mL^{-1} MTT, 3–4 h incubation), and absorbance read at 570 nm. Results (mean ± SD, $n \geq 3$) were normalized to untreated controls. The relative cell viability was determined (%) using the following equation:

$$\text{Cell viability} = \frac{OD\ sample}{OD\ control} \times 100\ \%$$

where OD sample is the absorbance of the test sample and OD control is the absorbance of control sample.

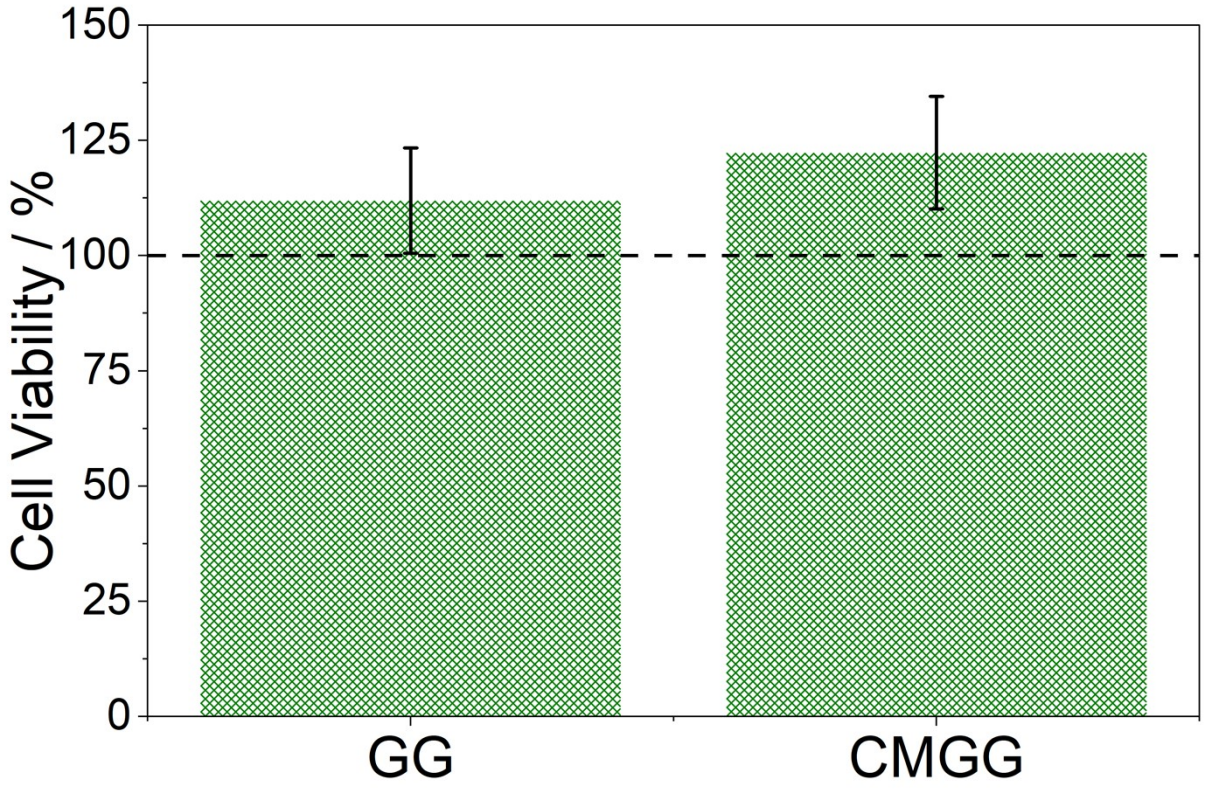

Figure S1. Cell viability (MTT assay) of human dermal fibroblasts exposed to GG an CMGG for 72 h. Data presented are mean ± SD of triplicate values.

Molecular Docking:

Molecular docking simulations were performed using Schrödinger Suite 2023-1 (Schrödinger, LLC, New York, NY, USA). The crystal structure of dihydropteroate synthase (DHPS) was obtained from the RCSB Protein Data Bank (PDB ID: 3TZF) [1].

Protein Preparation [2]:

The protein structure was pre-processed using the Protein Preparation Wizard in Maestro, which included assignment of bond orders, addition of missing hydrogen atoms, optimization of hydroxyl, amide, and thiol group orientations, removal of water molecules located >5 Å from

the bound ligand, protonation state adjustment using Epik (pH 7.0 ± 0.5) and restrained energy minimization with the OPLS4 force field (convergence threshold: 0.3 Å RMSD for heavy atoms).

Ligands were prepared using LigPrep with input files in .sdf or .mol2 format, ionization states generated with Epik (pH 7.0 ± 0.5), retention of chiral centres and energy minimization using the OPLS4 force field[3].

The receptor grid was generated using the Receptor Grid Generation module in Maestro[4] with the grid box centred on the co-crystallized ligand's centroid (PDB: 3TZF), inner grid box dimensions: 30 × 30 × 30 Å, van der Waals scaling factor: 1.0; partial charge cutoff: 0.25 and without any positional constraints applied.

Flexible molecular docking[5] was performed using Glide in Standard Precision (SP) mode with flexible ligand sampling and post-docking energy minimization applied, retention of up to 10 poses per ligand and pose scoring and ranking using the GlideScore function.

Docked poses were analysed for binding interactions[6], including hydrogen bonding, hydrophobic interactions and π–π stacking.

3D ligand–protein complexes were visualized and analysed using UCSF Chimera (v1.15), enabling evaluation of binding orientation and interaction geometry.

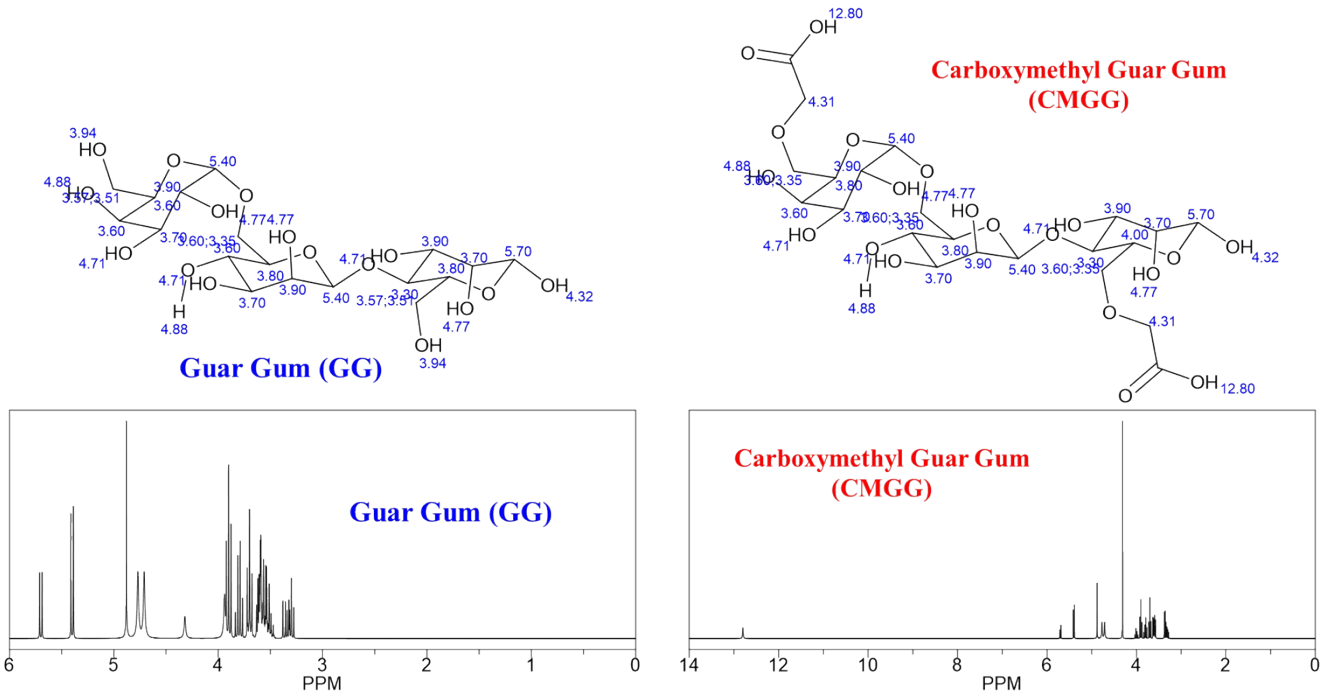

Figure S2. ^{1}H NMR spectra of unmodified GG (left) and carboxymethyl guar gum CMGG (right) monomers with all attributions, simulated using ChemDraw software.

Fourier Transform Infrared Spectroscopy (FTIR):

The structural and chemical modifications of GG through carboxymethylation were systematically analysed using FTIR spectroscopy, as shown in **Figure S2**. FTIR spectrum of unmodified GG (**Figure S2a**) a broad absorption band centred at 3315 cm^{-1} corresponds to the stretching vibrations of -O–H bonds. This band is characteristic of the extensive hydrogen bonding network formed by hydroxyl groups in the GG structure, indicative of its hydrophilic nature and alcohol functionalities [7]. Additionally, a distinct absorption band at 2914 cm^{-1} is observed, attributed to the asymmetric and symmetric stretching vibrations of sp^3 C–H bonds, reflecting the hydrocarbon framework within the polysaccharide matrix [8]. The spectrum also shows a characteristic band at 1641 cm^{-1}, typically associated with the bending vibrations of adsorbed water molecules (H-O-H). The hydrophilic nature of GG results in the retention of

moisture within its polymeric structure, leading to this prominent band [9] Another notable peak at 1372 cm^{-1} is assigned to the bending vibrations of -OH groups from primary alcohol functionalities, further underscoring the prevalence of hydroxyl groups. Additional structural details are evident in the region below 1200 cm^{-1}, where significant features of the GG backbone are observed. The absorption peak at 1148 cm^{-1} is attributed to asymmetric C–O stretching vibrations, while the strong and sharp band at 1016 cm^{-1} corresponds to C–O–C stretching vibrations, which are characteristic of glycosidic linkages in the GG molecular framework [10]. Moreover, low-frequency bands at 867 and 466 cm^{-1} are ascribed to skeletal vibrations, including C–H bending and other vibrational modes specific to polysaccharides [9].

FTIR spectrum of CMGG (**Figure S2b**) showed substantial changes, reflecting the structural modifications induced by the carboxymethylation process. An absorption band at 3158 cm^{-1} emerges, which can be attributed to enhanced hydrogen bonding interactions resulting from the introduction of carboxymethyl groups ($-CH_2-COO^-$). This band signifies the strengthening of intra- and inter-molecular hydrogen bonds within the modified polysaccharide network. Another notable feature is the appearance of a band at 2843 cm^{-1}, indicating an increased presence of $-CH_2-$ groups, which reflects the successful substitution of hydroxyl groups by carboxymethyl functionalities during the reaction. The distinct absorption band at 1725 cm^{-1} is associated with the stretching vibrations of >C=O bonds in carboxylic acid groups, providing definitive evidence for the chemical modification of GG to include carboxylic functionalities. Two additional prominent bands at 1587 and 1416 cm^{-1} are observed, corresponding to the asymmetric and symmetric stretching vibrations of carboxylate ions (COO^-), respectively. These bands are hallmark indicators of the successful incorporation of carboxymethyl groups into the GG structure, confirming the formation of carboxylate functionalities ($-CH_2-COO^-$). The relative intensity and clarity of these bands highlight the efficiency of the carboxymethylation reaction.

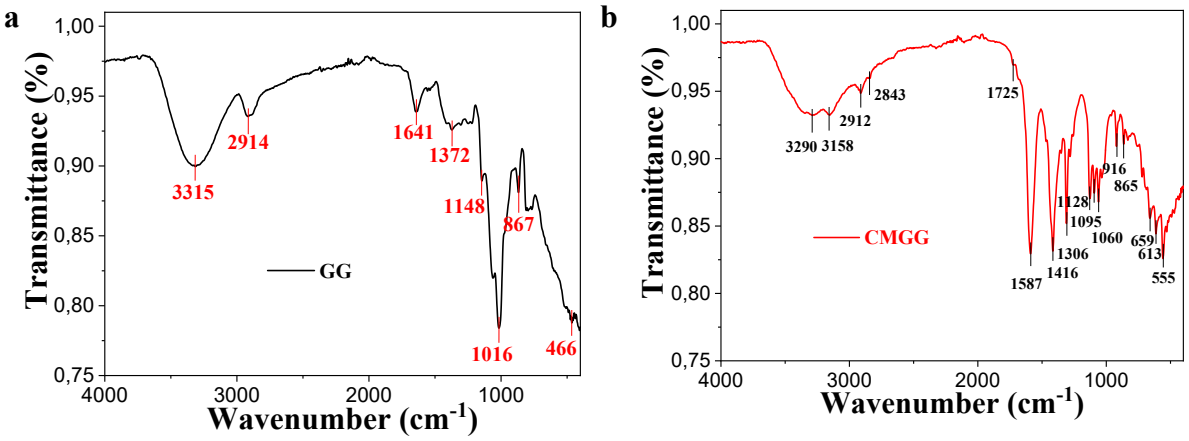

Figure S3. FTIR spectra of (a) unmodified GG and (b) carboxymethyl guar gum CMGG with full attribution.

Morphological analysis

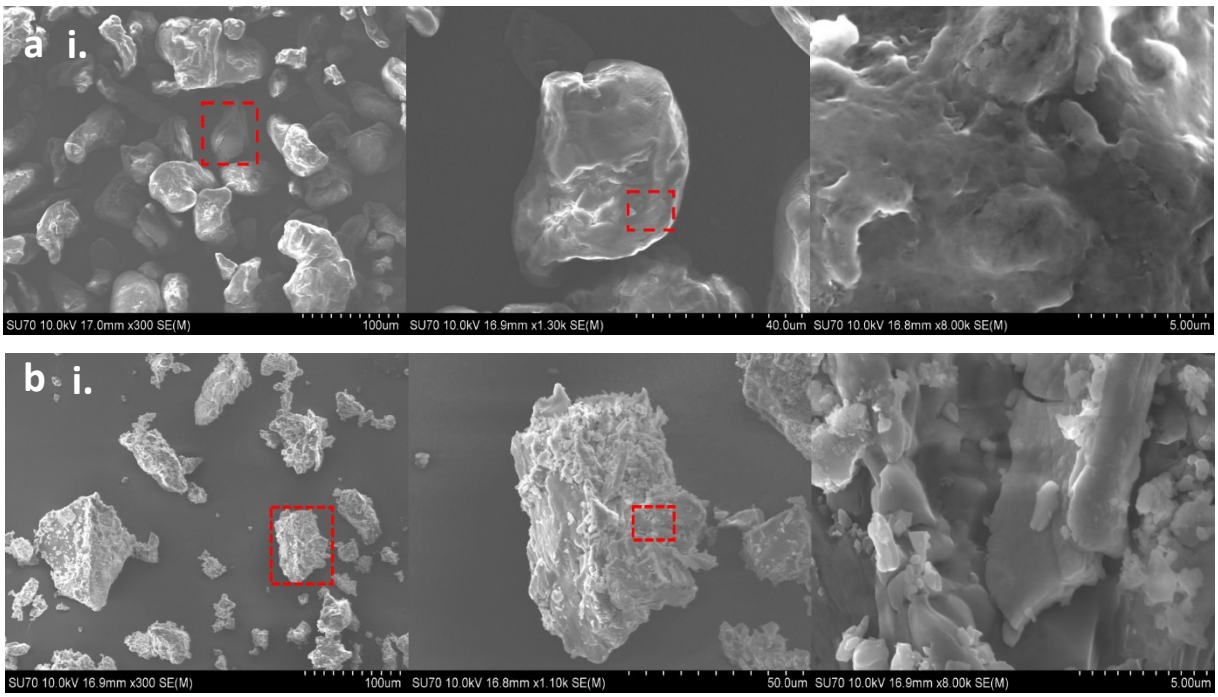

Figure S4. SEM images of (**a**, top) control without MCA (unmodified GG) and (**b**, bottom) CMGG after subsequently rinsing with deionized water, respectively. The red dashed squares

represent the region where higher magnification was executed. Scale bars are 100 µm (**i**, left), 50 µm (**ii**, centre) and 5µm (**iii**, right), respectively.

Thermogravimetric Analysis coupled with Differential Scanning Calorimetry (DSC):

The DSC thermograms (**Figures S4a** and **S4b**) further illustrate the impact of carboxymethylation on the thermal behaviour of GG. Unmodified GG exhibits a glass transition temperature (T_g) at 92°C, with multiple exothermic peaks at higher temperatures corresponding to glycosidic bond cleavage, oxidative decomposition, and carbonization. In contrast, CMGG presents a lower T_g at 56°C, but exhibited additional endothermic peaks at 148°C, 193°C, and 207°C indicate enhanced molecular organization and crystalline domain formation, likely stabilized by hydrogen bonding and electrostatic interactions. The observed exothermic peaks at 464°C and 605°C correspond to the degradation of modified polysaccharide chains and subsequent carbonization, reinforcing the improved thermal stability of CMGG.

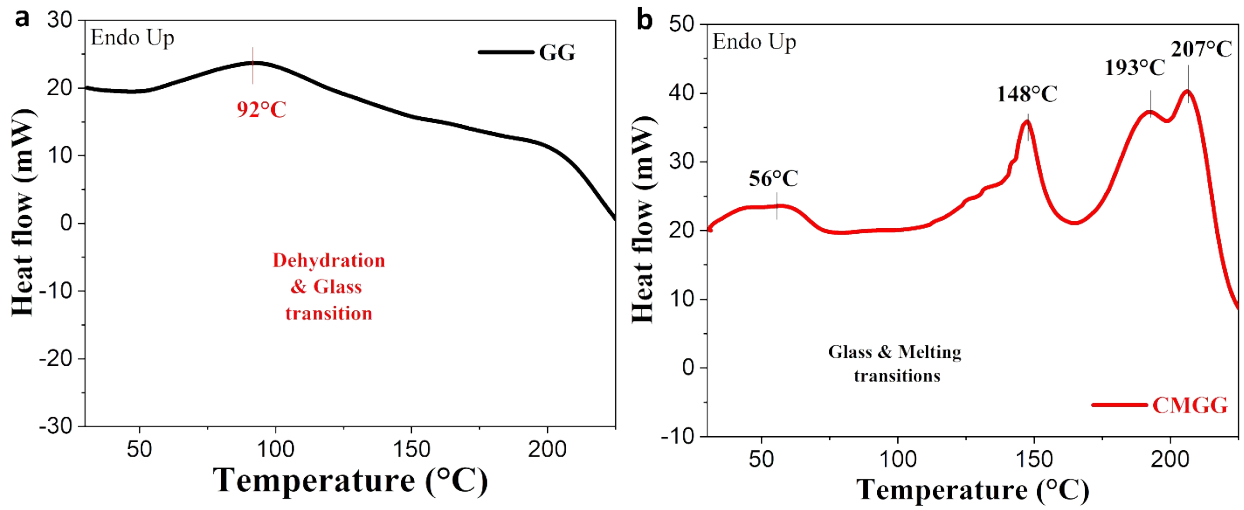

Figure S5. DSC profile for GG (**a**, black) and CMGG (**b**, red).

Table S2. Thermal properties of GG and CMGG obtained by TGA/DSC.

Samples	T_i (°C)	T_d(°C)	T_{max}(°C)	Residue at	T_m (°C)	ΔH°_m(J/g)

				600°C (%)		
GG	65 - 264	303	535	5	n.d.	n.d.
CMGG	95 - 249	265	668	15	148-193-207	841.6

Here, T_i is the temperature of initiation of degradation (°C), T_d is the temperature at the maximum rate of degradation (°C), T_{max} is the temperature of maximum weight loss (°C), T_m is the melting temperature (°C), and ΔH°_m is the enthalpy of melting (J/g).

Similarly, **Table S2** reveals a significantly higher melting enthalpy (ΔH°_m) for CMGG. This notable value, compared to the undetermined ΔH°_m for unmodified GG, highlights the enhanced crystalline network of CMGG. This improvement can be directly linked to the carboxymethylation process, which introduces functional groups that foster stronger intermolecular interactions, including hydrogen bonding and electrostatic forces. These interactions drive molecular alignment and the formation of ordered crystalline domains, thereby increasing the material's thermal stability and melting enthalpy. The lack of a detectable ΔH°_m for unmodified GG points to its predominantly amorphous nature, underlining the transformative effect of carboxymethylation on the polymer's structure.

Antibacterial Activity

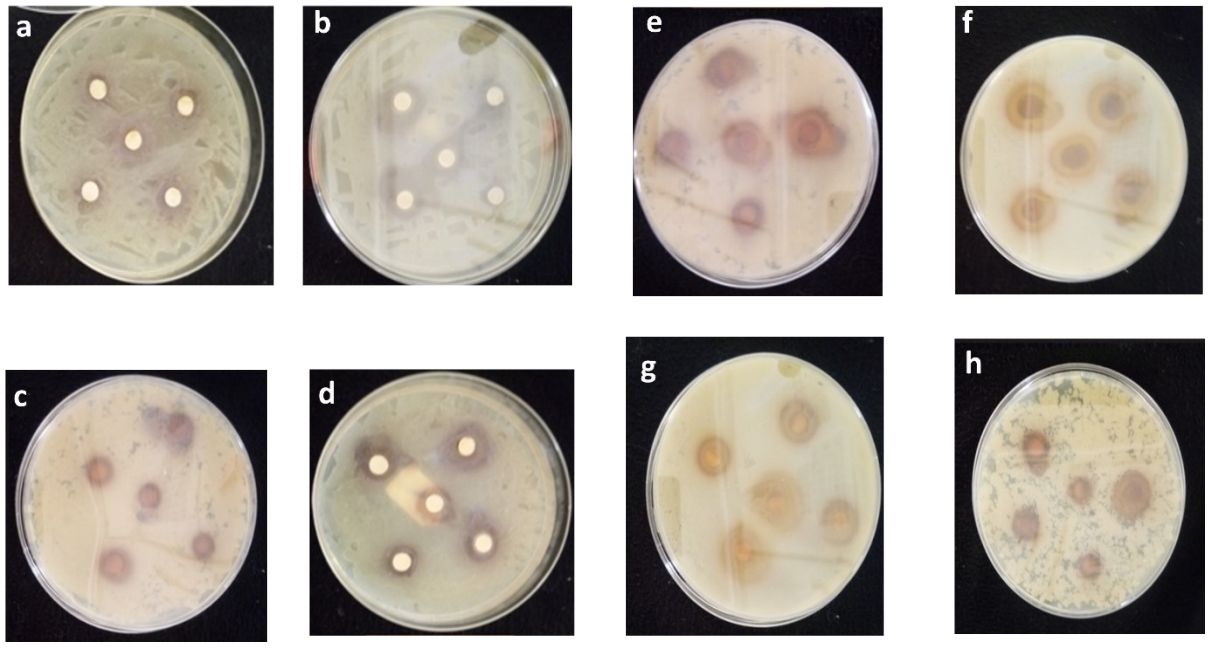

Figure S6. Representative pictures of the antibacterial essay for (a-d) GG and (e-h) CMGG. a, e are *Bacillus cereus*, b, f are *Streptococcus thermophilus*, c, g are *Escherichia coli* and d, h are *Staphylococcus aureus*, respectively.

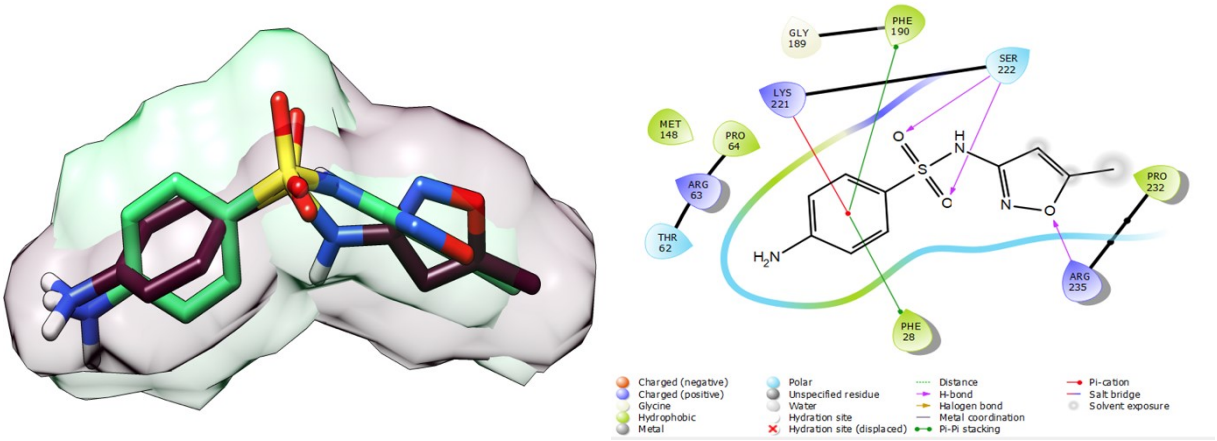

Figure S7. Calculated structure of the co-crystallized ligand (sulfamethoxazole) (left) and result of the molecular re-docked position of the co-crystallized ligand (less than 1 Å), interacting with groups of the DHPS enzyme (right).

References

[1] H.M. Berman, The Protein Data Bank, Nucleic Acids Res 28 (2000) 235–242. https://doi.org/10.1093/nar/28.1.235.

[2] G. Madhavi Sastry, M. Adzhigirey, T. Day, R. Annabhimoju, W. Sherman, Protein and ligand preparation: parameters, protocols, and influence on virtual screening enrichments, J Comput Aided Mol Des 27 (2013) 221–234. https://doi.org/10.1007/s10822-013-9644-8.

[3] Schrödinger Release 2023-1: LigPrep, (2023).

[4] Schrödinger Release 2023-1: Maestro, (2023).

[5] R.A. Friesner, J.L. Banks, R.B. Murphy, T.A. Halgren, J.J. Klicic, D.T. Mainz, M.P. Repasky, E.H. Knoll, M. Shelley, J.K. Perry, D.E. Shaw, P. Francis, P.S. Shenkin, Glide: A New Approach for Rapid, Accurate Docking and Scoring. 1. Method and Assessment of Docking Accuracy, J Med Chem 47 (2004) 1739–1749. https://doi.org/10.1021/jm0306430.

[6] E.F. Pettersen, T.D. Goddard, C.C. Huang, G.S. Couch, D.M. Greenblatt, E.C. Meng, T.E. Ferrin, UCSF Chimera—A visualization system for exploratory research and analysis, J Comput Chem 25 (2004) 1605–1612. https://doi.org/10.1002/jcc.20084.

[7] J.Y. Xin, Y. Wang, T. Liu, K. Lin, L. Chang, C.G. Xia, Biosysthesis of corn starch palmitate by lipase novozym 435, Int J Mol Sci 13 (2012) 7226–7236. https://doi.org/10.3390/ijms13067226.

[8] C. Pozo, S. Rodríguez-Llamazares, R. Bouza, L. Barral, J. Castaño, N. Müller, I. Restrepo, Study of the structural order of native starch granules using combined FTIR and XRD analysis, Journal of Polymer Research 25 (2018). https://doi.org/10.1007/s10965-018-1651-y.

[9] G. Dodi, A. Pala, E. Barbu, D. Peptanariu, D. Hritcu, M.I. Popa, B.I. Tamba, Carboxymethyl guar gum nanoparticles for drug delivery applications: Preparation and preliminary in-vitro investigations, Materials Science and Engineering C 63 (2016) 628–636. https://doi.org/10.1016/j.msec.2016.03.032.

[10] K.K. Mali, S.C. Dhawale, R.J. Dias, Synthesis and characterization of hydrogel films of carboxymethyl tamarind gum using citric acid, Int J Biol Macromol 105 (2017) 463–470. https://doi.org/10.1016/j.ijbiomac.2017.07.058.